

# RIS-Jamming: Breaking Key Consistency in Channel Reciprocity-based Key Generation

Guyue Li, *Member, IEEE*, Paul Staat, Haoyu Li, Markus Heinrichs, Christian Zenger *Member, IEEE*, Rainer Kronberger, Harald Elders-Boll, Christof Paar *Fellow, IEEE* and Aiqun Hu, *Senior Member, IEEE*

**Abstract**—Channel Reciprocity-based Key Generation (CRKG) exploits reciprocal channel randomness to establish shared secret keys between wireless terminals. This new security technique is expected to complement existing cryptographic techniques for secret key distribution of future wireless networks. In this paper, we present a new attack, reconfigurable intelligent surface (RIS) jamming, and show that an attacker can prevent legitimate users from agreeing on the same key by deploying a malicious RIS to break channel reciprocity. Specifically, we elaborate on three examples to implement the RIS jamming attack: Using active nonreciprocal circuits, performing time-varying controls, and reducing the signal-to-noise ratio. The attack effect is then studied by formulating the secret key rate with a relationship to the deployment of RIS. To resist such RIS jamming attacks, we propose a countermeasure that exploits wideband signals for multipath separation. The malicious RIS path is distinguished from all separated channel paths, and thus the countermeasure is referred to as contaminated path removal-based CRKG (CRP-CRKG). We present simulation results, showing that legitimate users under RIS jamming are still able to generate secret keys from the remaining paths. We also experimentally demonstrate the RIS jamming attack by using commodity Wi-Fi devices in conjunction with a fabricated RIS prototype. In our experiments, we were able to increase the average bit disagreement ratio (BDR) of raw secret keys by 20%. Further, we successfully demonstrate the proposed CRP-CRKG countermeasure to tackle RIS jamming in wideband systems as long as the source of randomness and the RIS propagation paths are separable.

**Index Terms**—Physical layer security, secret key generation, reconfigurable intelligent surface, channel reciprocity.

## I. INTRODUCTION

The steady growth in connectivity, fueled by the advent of electronic-commerce applications and the ubiquity of wireless communications, has led to an unprecedented awareness of the importance of network security in all its guises [1]. In the realm of wireless security, traditional cryptographic schemes

are used to secure communications, i.e., symmetric and public-key schemes. However, these schemes involve additional effort for, e.g., a public-key infrastructure, key sharing, or key management. Further, the loss and theft of encryption keys pose additional risks. Finally, especially for asymmetric schemes, the notion of computational security is weakened by the development of efficient algorithms as well as the increase in computational power of modern computers (e.g., quantum computers).

In this context, Channel Reciprocity-based Key Generation (CRKG) has emerged as a promising technique to complement existing cryptographic techniques for secure key sharing. The technique is developed on the source model of physical-layer security [2], where two legitimate terminals observe a common random source that is inaccessible to an eavesdropper. Such a natural shared entropy source exploited by CRKG is the wireless fading channel [3]. Suppose that a pair of wireless terminals communicate with each other on the same frequency in a wireless communication environment. The wireless channel between two terminals produces a random mapping between the transmitted and received signals. This mapping, known as channel state information (CSI), changes with time in a manner that is location-specific and reciprocal, i.e., the mapping is essentially the same in both directions. Hence, if both terminals possess some means of observing the fading of their mutual channel at approximately the same time, their resulting observations are highly statistically dependent. For example, in time-division duplex (TDD) systems, when the coherence time of the channel is sufficiently long, these mutual channels are approximately identical. Additionally, this time-varying mapping decorrelates completely over distances of the order of a few wavelengths. During the past thirty years, much work has been devoted to theoretical study as well as to prototype implementation of CRKG under various wireless communication protocols.

Compared with cryptographic techniques, CRKG does not require that the attacker has limited computational capability [4]. On the other hand, CRKG relies on the reciprocity of wireless channels. That is, even partially non-reciprocal radio channels can cause a severe mismatch in the generated key material, resulting in the failure of the CRKG procedure. According to the Rayleigh-Carson reciprocity theorem [5], channel reciprocity holds if and only if the material tensors of the transmission media and scatterers, such as air, ground, and walls, are symmetric for the uplink and the downlink. Although natural wireless channels have the inherent and fundamental property of channel reciprocity, recent research

Guyue Li and Haoyu Li are with the School of Cyber Science and Engineering, Southeast University, Nanjing 210096, China (e-mail: guyuelee@seu.edu.cn; haoyuli@seu.edu.cn).

Paul Staat and Christof Paar are with Max Planck Institute for Security and Privacy, Bochum, Germany (e-mail: paul.staat@mpi-sp.org; christof.paar@mpi-sp.org).

Markus Heinrichs, Rainer Kronberger, and Harald Elders-Boll are with TH Köln – University of Applied Sciences, Cologne, Germany (e-mail: markus.heinrichs@th-koeln.de; rainer.kronberger@th-koeln.de; harald.elders-boll@th-koeln.de).

Christian Zenger is with PHYSEC GmbH, Bochum, Germany and Ruhr University Bochum, Germany (e-mail: christian.zenger@rub.de).

Aiqun Hu is with the National Mobile Communications Research Laboratory, Southeast University, Nanjing 210096, China (e-mail: aqhu@seu.edu.cn).

Guyue Li and Aiqun Hu are also with the Purple Mountain Laboratories for Network and Communication Security, Nanjing 210096, China.

on the emerging topic of reconfigurable intelligent surface (RIS) has found that the artificial electromagnetic characteristics of RIS do not strictly follow the normal laws of nature [6], [7]. RIS is a kind of artificial surface that consists of a large number of sub-wavelength unit cells with tunable electromagnetic responses, including phase, amplitude, and polarization [8]. When an RIS participates in the process of CRKG, the effective channel is the superimposition of the direct link and the RIS-induced link, the latter of which is given by the product of two physical channel gains and the RIS gain. The success of CRKG, in this context, is also affected by the reciprocity of the RIS-induced link. In [6], the authors show that the reciprocity of the RIS-induced link is not unconditional. For example, the RIS should have a symmetric structure and circuit, and its reflection coefficient matrix should be the same in both directions. In other words, the reciprocity property of the entire channel could be destroyed by deploying a malicious RIS that does not satisfy these conditions. In this paper, we define such kind of attack as *RIS jamming attack*, as the reciprocal direct link is jammed by the RIS-induced link intentionally. As an RIS is considered to be nearly passive, this attack differs from existing jamming attacks [9], thereby urging a new model to study its effect and a reconsideration of the countermeasure.

This paper aims to address the security problem of CRKG in wireless communication systems in the presence of a malicious RIS. To study the destructive effect, we formulate a general RIS-involved model, identify three ways to realize the RIS jamming attack, and derive the resulting reduction of the secret key rate. To mitigate the potential severity of this attack, we propose a new scheme for sustaining secret key generation. More specifically, the main contributions of this paper are listed as follows.

- We propose a new kind of attack to CRKG, RIS jamming, and show that an attacker can prevent legitimate users from agreeing on the same key by deploying one or multiple malicious RISs to break channel reciprocity. In particular, we introduce three examples to realize the RIS jamming attack, including using active nonreciprocal circuits, performing out-of-sync controls, and reducing signal-to-noise ratio (SNR).
- We analyze the attack effect of RIS jamming by formulating the secret key rate with a relationship of the deployment of RIS. To resist such RIS jamming attacks, we propose a countermeasure that exploits the wideband signals for multipath separation and then distinguishes the malicious path from all separated channel paths. Consequently, even in such difficult circumstances, it is still possible for legitimate users to generate secret keys by taking care of channel gains from the remaining paths.
- We verify the effectiveness of RIS jamming attacks and its countermeasure through both simulations and experiments. Numerical simulation and experimental results are consistent, and they substantiate the statement that RIS jamming attacks have a non-negligible negative effect on BDR and the proposed CPR-CRKG scheme can mitigate their impacts in wideband systems.

## II. RELATED WORKS

An RIS is capable of creating an intelligent reconfigurable propagation environment. Thus, besides improving wireless communication, the RIS technology likewise has significant potential in view of CRKG [10], [11]. When the RIS is controlled by legitimate users, it can introduce an additional reciprocal channel path and enhance the temporal fluctuation of channel measurements. As a result, over the past three years, RIS has been considered a helper to assist CRKG in boosting the secret key generation rate.

With an elaborate design of RIS configuration, the secret key generation rate can be largely improved [12]–[16]. Ji *et al.* randomly changes the phase of RIS to introduce artificial randomness and increase the key generation rate (KGR) [12]. In another work [13], the same authors optimize RIS reflecting coefficients to maximize the lower bound of the secret key rate in scenarios of multiple eavesdroppers. Moreover, Lu *et al.* adjusted the placement of RIS to maximize the key rate capacity [15]. In [14], the authors optimized the RIS reflecting coefficients to maximize the key generation rate and minimize transmit power while guaranteeing the key generation rate target. Wei *et al.* in [16] further studied the effect of RIS on CRKG under the pilot spoofing attack. RIS also makes it possible to yield secret keys from wireless channels in some harsh propagation scenarios, e.g., wave-blockage environments [17] and static or low-entropy environments [18]–[20], extending the application range of PKG. In [17], the authors proposed an RIS-assisted multi-user key generation scheme that optimizes the configuration of the RIS to maximize the sum secret key rate between an access point and multiple users over independent and correlated fading channels. Jiao *et al.* increased the randomness of the wireless channel by rapidly changing the RIS configurations and proposed a machine learning-based adaptive quantization level prediction scheme to decide an optimal quantization level based on channel state information CSI [19]. The authors in [18] also used an RIS to boost the secret key rate in quasi-static environments and found that the secret key rate is determined by the number of RIS elements, the correlation coefficient, the pilot length and the quality of the reflecting channel. The first field studies of RIS-assisted CRKG with an OFDM system were demonstrated by Staat *et al.* in [20]. Their prototype system achieved a key generation rate (KGR) of 97.39 bps with 6.5% bit disagreement ratio (BDR) after quantization while passing standard randomness tests in a static environment.

However, previous works rarely considered that RIS could likewise be controlled by an attacker. In the context of disrupting wireless communications, Staat *et al.* demonstrated how an RIS can disrupt Wi-Fi networks [21]. In the context of CRKG, we have partially investigated an example of the RIS jamming attack in our previous work [22]. However, its attack model is not general and no field verification has been provided. It is yet to be explored, how this attack impacts CRKG in practical scenarios and how to withstand this attack. To bridge these gaps, this paper carries out a comprehensive study of the RIS jamming attack in the field of CRKG from both theoretical and experimental aspects.

### III. SYSTEM MODEL

In this section, we build a general model for the scenario where an RIS participates in the CRKG process. On this basis, we give the problem statement.

#### A. RIS-involved Channel Model

Fig. 1 depicts the RIS-involved CRKG scenario considered in this paper, considering three parties. Alice and Bob are two legitimate terminals that seek to establish a shared cryptographic key from their channel observations. For simplicity, they are assumed to be equipped with a single antenna and deploy a standard TDD wireless communication protocol, e.g., IEEE 802.11n Wi-Fi with orthogonal frequency-division multiplexing (OFDM) for bi-directional communications. Eve is an attacker who is aware of the key generation procedure of Alice and Bob. The distance between Eve and Alice/Bob is several orders of magnitude larger than the wavelength, and thus Eve's channel observations are assumed to be independent of those of Alice and Bob. In order to accomplish the purpose of interrupting the CRKG procedure, Eve places a malicious RIS device between Alice and Bob to partially control the wireless propagation channel. To illustrate this effect, we consider a simplified 2D system setup, as shown in Fig. 1, where Alice and Bob are located on a line with horizontal distance  $D$  m, and the RIS device is deployed on a line  $H$  m above Alice and Bob. The horizontal distance between the RIS and Alice is denoted by  $d_{ar}$ . Accordingly,  $d_{rb} = D - d_{ar}$  represents the horizontal distance between the RIS and Bob. The RIS consists of  $M = M_x \times M_y$  reflecting elements of size  $d_x \times d_y$ . Each reflecting element is an electrically-small low-gain element embedded on a substrate.

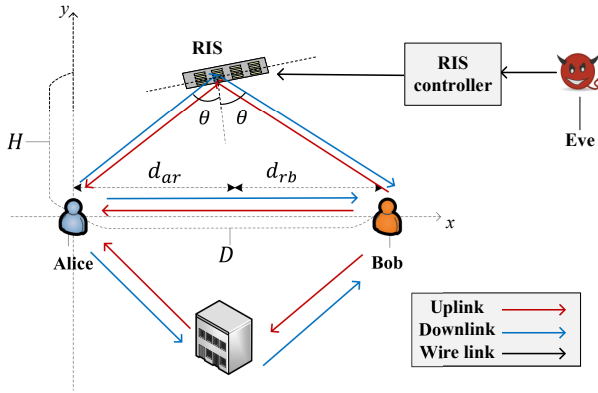


Fig. 1: System model of the RIS-involved CRKG scenario.

In general, the total channel between Alice and Bob is the superposition of the direct link and the RIS-induced link. Accordingly, we elaborate on the model of these two links below. First, regarding the direct link, we suppose that it has  $L$  propagation paths, and its channel impulse response can be expressed as

$$g_d(\tau) = \sum_{\ell=1}^L \alpha_{\ell} \delta(\tau - \tau_{\ell}), \quad (1)$$

where  $\alpha_{\ell} \in \mathbb{C}$  and  $\tau_{\ell} \in \mathbb{R}$  are the complex channel gain and the time delay of the  $\ell$ -th path, respectively. The statistical power gain of each path,  $\beta_{\ell}$ , is decided by the path loss, which can be modeled as

$$\beta_{\ell} = \mathbb{E}\{\alpha_{\ell} \alpha_{\ell}^*\} = 1/d_{\ell}^2, \quad (2)$$

where  $d_{\ell}$  is the distance of the  $\ell$ -th path. Hence, its channel frequency response on the  $k$ -th subcarrier can be expressed as

$$h_d(k) = \sum_{\ell=1}^L \alpha_{\ell} e^{-j2\pi\tau_{\ell}k/K}, k \in \{1, 2, \dots, K\}, \quad (3)$$

where  $K$  is the number of subcarriers.

Second, the channel impulse response of the RIS-induced channel is modeled as

$$h_r(\tau) = \mathbf{h}_{ar}^T \mathbf{\Lambda} \mathbf{h}_{rb} \delta(\tau - \tau_r), \quad (4)$$

where  $\tau_r$  is the time delay of the RIS path,  $\mathbf{h}_{ar} \in \mathbb{C}^{M \times 1}$  and  $\mathbf{h}_{rb} \in \mathbb{C}^{M \times 1}$  denote the channel coefficient vector from Alice to the RIS and the channel coefficient vector from the RIS to Bob,  $\mathbf{\Lambda} = \text{Diag}(\lambda_1, \lambda_2, \dots, \lambda_M)$  is a diagonal matrix, representing RIS' signal reflection. The elements of  $\mathbf{\Lambda}$  are the equivalent reflection coefficients of each unit cell. Its  $i$ -th diagonal element is modeled as follows:

$$\lambda_i = a_i e^{j\Phi_i}, i = 1, 2, \dots, M. \quad (5)$$

where  $a_i$  and  $\Phi_i$  correspond to the amplitude response and the phase response, respectively. Here,  $a_i$  and  $\Phi_i$  can be adjusted by a smart controller, e.g., a microcontroller or a field-programmable gate array (FPGA).

In (4), the power gain of the RIS path is given by

$$\beta_r = \mathbb{E}\{(\mathbf{h}_{ar}^T \mathbf{\Lambda} \mathbf{h}_{rb})(\mathbf{h}_{ar}^T \mathbf{\Lambda} \mathbf{h}_{rb})^*\} = \beta |\Gamma \cos(\theta)|^2 / d_r^2, \quad (6)$$

where  $\beta = \mathbb{E}\{a_i a_i^*\}$  indicates the power of RIS units,  $d_r$  is the distance of RIS path,  $\theta$  is the incident angle.  $\Gamma$  is the Fresnel reflection coefficient, which can be modeled as [23]

$$\Gamma = \frac{\epsilon_r \cos \theta - \sqrt{\epsilon_r - \sin^2 \theta}}{\epsilon_r \cos \theta + \sqrt{\epsilon_r - \sin^2 \theta}}, \quad (7)$$

where  $\epsilon_r$  denotes the relative permittivity of the reflecting medium. For simplicity, we assume that all reflection units have the same  $\beta$  and  $\Gamma$ . By adding a power amplifier,  $\beta$  can be magnified.

To sum up, the total channel impulse response can be expressed as

$$h(\tau) = \sum_{\ell=1}^L \beta_{\ell} \delta(\tau - \tau_{\ell}) + \mathbf{h}_{ar}^T \mathbf{\Lambda} \mathbf{h}_{rb} \delta(\tau - \tau_r) \quad (8)$$

and channel frequency response between Alice and Bob is given by

$$h(k) = h_d(k) + \mathbf{h}_{ar}^T \mathbf{\Lambda} \mathbf{h}_{rb} e^{-j2\pi\tau_r k/K}. \quad (9)$$

By stacking these channel frequency responses of all subcarriers together, we obtain the entire channel vector of

$$\mathbf{h} = [h(1), h(2), \dots, h(K)]^T. \quad (10)$$

## B. Process of CRKG

In the process of CRKG, Alice and Bob first exchange known OFDM symbols as probe signals to gather channel parameters. Each party can then use the received signal along with the probe signal to compute an estimate  $\hat{\mathbf{h}}$  of  $\mathbf{h}$ . For simplicity, we assume that all the above physical channels are block-fading. For the  $k$ -th subcarrier, its channel frequency response at time  $t$  is given by

$$h(k, t) = \sum_{n=-\infty}^{\infty} h_n(k)x(t - nT_c), \quad (11)$$

where  $h_n(k)$  is the channel frequency response for the  $n$ -th block and  $x(t)$  is a rectangular wave

$$x(t) = \begin{cases} 1, & nT_c \leq t < (n+1)T_c, \\ 0, & \text{otherwise,} \end{cases} \quad (12)$$

and  $T_c$  is the channel coherence time.

In a TDD system, Alice waits to receive a probe signal from Bob before responding with a probe signal and vice-versa. Assume that Alice and Bob transmit pilot signals at  $t_1$  and  $t_2$ , respectively, the received signal at Bob and Alice at the  $k$ -th subcarrier can be written as

$$\begin{aligned} y_{ab}(k, t_1) &= h(k, t_1)s(t_1) + n_b(k, t_1), \\ y_{ba}(k, t_2) &= h(k, t_2)s(t_2) + n_a(k, t_2), \end{aligned} \quad (13)$$

where  $s(t_1)$  and  $s(t_2)$  denote the known probe signal,  $n_b(k, t_1)$  and  $n_a(k, t_2)$  are the independent additive white Gaussian noise (AWGN) processes at Bob and Alice. In this paper, the SNR is defined as the ratio of pilot signal power to noise power.

Using the received signal, Bob and Alice utilize a least-squares (LS) channel estimation:

$$\begin{aligned} \tilde{h}_{ab}(k, t_1) &= \mathbf{h}_{ar}^T(t_1)\mathbf{\Lambda}(t_1)\mathbf{h}_{rb}(t_1)e^{-j2\pi\tau_r(t_1)k/K} \\ &\quad + h_d(k, t_1) + z_b(k, t_1), \\ \tilde{h}_{ba}(k, t_2) &= \mathbf{h}_{rb}^T(t_2)\mathbf{\Lambda}(t_2)\mathbf{h}_{ar}(t_2)e^{-j2\pi\tau_r(t_2)k/K} \\ &\quad + h_d(k, t_2) + z_a(k, t_2), \end{aligned} \quad (14)$$

where  $\mathbf{\Lambda}(t_2)$  is the RIS coefficients at time  $t_2$ , which is independent from  $\mathbf{\Lambda}(t_1)$ . The statistical gain of the RIS path at  $t_2$  is  $\beta_{r'}$ .  $z_b(k, t_1)$  and  $z_a(k, t_2)$  in (14) represent the AWGN terms due to  $n_b(k, t_1)$  and  $n_a(k, t_2)$  after processing by the function that estimates  $h$ . They both have a variance of  $\sigma^2$  so that the SNR is equal to  $1/\sigma^2$ .

In one channel probing round, the time difference  $t_2 - t_1$  is smaller than  $T_c$ , guaranteeing a high correlation of the channel observations. After channel probing, these channel estimates are then translated into identical bit-strings suitable for use as cryptographic keys. Since the channel estimates are continuous random variables, Alice and Bob first quantize them into raw keys using single-bit CDF quantization [24]. Next, the information reconciliation and privacy amplification procedures are used to generate identical and private secret keys. These steps are similar to existing works in the field of CRKG and are thus not particularly designed in this paper. We refer the interested reader to [25]–[28].

## C. Problem Statement

According to the above system model, the entire channel is partially under the control of Eve. Previous research indicates that the artificial electromagnetic characteristics of RISs do not strictly follow the normal laws of reciprocity [6]. As a result, Eve is able to obstruct the secret key agreement of CRKG by reducing the similarity of the legitimate bidirectional channel estimates. Although this attack idea is initially formed, more problems need to be investigated:

- How to design or control an RIS to realize this kind of attack in practice?
- How much of an impact can Eve have on the CRKG between Alice and Bob?
- Is it possible for Alice and Bob to mitigate the potential severity of this attack?

The rest of this paper will seek solutions to these questions from both theoretical and experimental aspects.

## IV. RIS JAMMING ATTACK

In this section, we first describe the basic idea of the RIS jamming attack and then elaborate on three implementation examples.

### A. Idea Description

Regarding the system model as described in Fig. 1, the success of CRKG relies on the reciprocity of  $\tilde{h}_{ab}(t_1, k)$  and  $\tilde{h}_{ba}(t_2, k)$ . When their reciprocity is weak, the BDR of the raw key becomes high. In this situation, correcting the errors via information reconciliation results in a great burden by the high computation cost and significant information leakage of the secret key. Typically, it is difficult to obtain identical key material with CRKG if the BDR of the raw key is larger than 20%. Building on this observation, an RIS jamming attack may obstruct the CRKG between Alice and Bob in two ways.

- *Breaking the reciprocity of the RIS-induced link:* As observed from (14), the reciprocity of the channel estimates depends on the reciprocity of the direct link as well as the RIS-induced link. If Alice and Bob send probes to one another at a fast enough rate, i.e., if  $T_p = t_2 - t_1$  is small, the physical channels between Alice and Bob at  $t_1$  and  $t_2$  can be highly correlated. The time delays are assumed to be the same. However, this high correlation is not guaranteed for  $\mathbf{\Lambda}(t_1)$  and  $\mathbf{\Lambda}(t_2)$  as these RIS-related parameters are under the control of Eve. In other words, Eve can reduce the correlation of  $\mathbf{\Lambda}(t_1)$  and  $\mathbf{\Lambda}(t_2)$  by applying intentional changes of the RIS response at time instants  $t_1$  and  $t_2$ .
- *Reducing the SNR of the entire channel:* The reciprocity of the entire channel estimates is also affected by the SNR due to the independent noise terms  $z_a(k, t_2)$  and  $z_b(k, t_1)$  in (14). Thus, another approach for Eve to break key agreement is to build an RIS-induced link that can suppress the direct link. In this scenario, the reciprocal channel is submerged by noise and thus makes it difficult to reach key agreement. In the worst case, the RIS-induced channel cancels the direct channel, leaving only independent noise in the channel estimates.

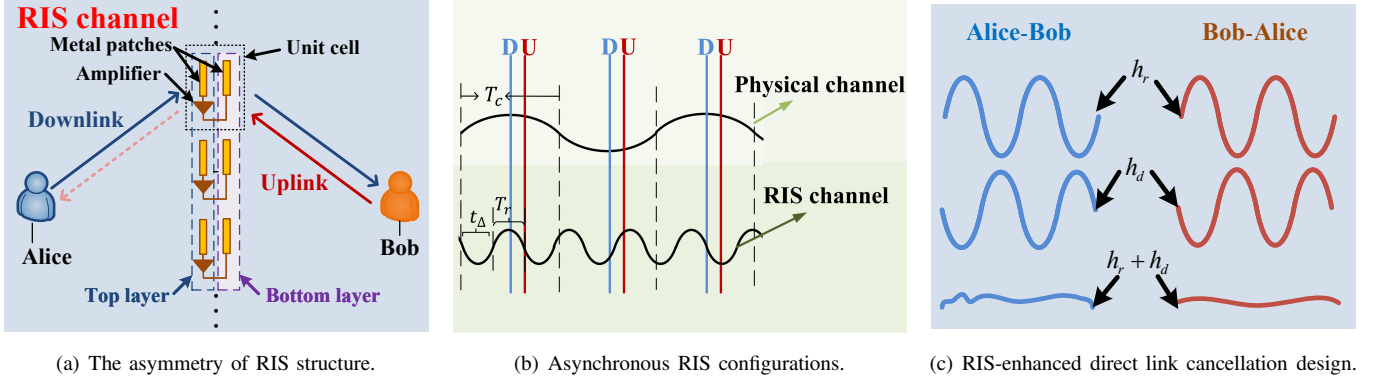


Fig. 2: Illustrations of the three RIS jamming attacks.

In both cases, the reciprocity of  $\tilde{\mathbf{h}}_{ab}(t_1)$  and  $\tilde{\mathbf{h}}_{ba}(t_2)$  will be disrupted due to the RIS operation. For this reason, we define such kind of attack as an RIS jamming attack in this paper.

### B. Attack Realization

Next, we elaborate on three examples of the RIS jamming attack. The first two of them aim at breaking the reciprocity of the RIS-induced link, while the last one intends to reduce the SNR of the entire channel.

1) *Asymmetry of RIS Structures*: The first way of implementing an RIS jamming attack makes use of the asymmetry of the RIS structure to cause different RIS signal reflection matrices in forward and reverse channels. That is, the response of an RIS unit cell can vary with the angle of incidence, thus yielding a non-reciprocal response [29]. Further, RIS unit cells could be deliberately designed to behave non-reciprocal, e.g., by utilizing active non-reciprocal circuits such as microwave amplifiers or isolators.

For example, as depicted in Fig. 2(a), in the forward direction of the RIS-induced link at time  $t_1$ , wireless signals are first captured by the metal patches on the RIS's top layer and transformed into circuit signals. After passing through amplifiers, the circuit signals are then radiated into space again by the metal patches on RIS's bottom layer. In the reverse direction at time  $t_2$ , however, due to the non-reciprocity of integrated amplifiers, the signals captured by the metal patches on RIS's bottom layer are isolated. In this case, the channels estimated at Bob and Alice are mathematically given by

$$\begin{aligned}\tilde{\mathbf{h}}_{ab}(k, t_1) &= \mathbf{h}_{ar}^T(t_1)\mathbf{\Lambda}(t_1)\mathbf{h}_{rb}(t_1)e^{-j2\pi\tau_r k/K} \\ &\quad + h_d(k, t_1) + z_a(k, t_1), \\ \tilde{\mathbf{h}}_{ba}(k, t_2) &= h_d(k, t_2) + z_b(k, t_2).\end{aligned}\quad (15)$$

As observed,  $\tilde{\mathbf{h}}_{ba}(k, t_2)$  differs from  $\tilde{\mathbf{h}}_{ba}(k, t_1)$ , mainly due to the isolation of its RIS-induced link, i.e.,  $\mathbf{\Lambda}(t_2) = 0$ .

2) *Asynchronous RIS Configurations*: The second method intends to make the channel observations of Alice and Bob non-reciprocal rather than introducing an actually non-reciprocal RIS link. For this, Eve takes advantage of asynchronous RIS configurations. Here, Eve randomly configures the RIS to adjust  $\mathbf{\Lambda}$  at a frequency of  $f_r$ . In other words, the reflection coefficients of the RIS remain constant within a time

block of  $T_r = 1/f_r$ . Then, the equivalent reflection coefficient of the  $i$ -th unit cell of the RIS at time  $t$  is given by

$$\lambda_i(t) = \sum_{n=-\infty}^{\infty} \lambda_{i,n} x'(t - nT_r + t_\Delta), \quad (16)$$

where  $\lambda_{i,n}$  is the equivalent reflection coefficient for the  $n$ -th time block and  $x'(t)$  is also a rectangular wave

$$x'(t) = \begin{cases} 1, & nT_r \leq t < (n+1)T_r, \\ 0, & \text{otherwise,} \end{cases} \quad (17)$$

and  $t_\Delta$  is the initial temporal deviation between  $\lambda_i$  and the physical channel. When  $T_r = T_c$  and  $t_\Delta = 0$ , change in RIS is synchronized with the change of physical channels. In this case,  $\mathbf{\Lambda}(t_1) = \mathbf{\Lambda}(t_2)$ , which will not have negative effects on CRKG. Conversely, if  $T_r < T_c$  or  $t_\Delta \neq 0$ ,  $\mathbf{\Lambda}(t_1)$  will be different from  $\mathbf{\Lambda}(t_2)$  with high probability. Accordingly, as illustrated in Fig. 2(b), Eve can realize the asynchronism by accelerating the switching frequency of the RIS, introducing a considerable temporal deviation, or both. In either case,  $t_1$  and  $t_2$  fall into different time block, so that  $\mathbf{\Lambda}(t_1)$  will be independent from  $\mathbf{\Lambda}(t_2)$ , which reduces the similarity between  $\tilde{\mathbf{h}}_{ba}(k, t_2)$  and  $\tilde{\mathbf{h}}_{ba}(k, t_1)$ .

3) *RIS-enhanced Direct Link Cancellation Design*: Another example of the RIS jamming attack in CRKG is direct link cancellation, where the reflected channel and the direct channel can be destructively combined, as shown in Fig. 2(c). However, this example requires that Eve knows not only the channel from Alice/Bob to the RIS, but also the direct link between Alice and Bob, which is a strong assumption in practice. Additionally, once Eve knows the direct link between Alice and Bob, after weighing the advantages and disadvantages, she would prefer to steal the secret key insensibly rather than destroy the key generation.

Table I summarizes the above three examples of the RIS jamming attack from the aspects of technical means, requirement, destructiveness, and implementation. Considering the last example has strict requirements for implementation, the rest of this paper is focused on the first two examples.

TABLE I: Three examples of the RIS jamming attack.

	Technical means	Requirement	Destructiveness	Implementation
1	Asymmetric RIS structure	Active non-reciprocal circuits on RIS	Middle	Middle
2	Asynchronous RIS configuration	Fast switching speed of RIS configurations	Strong	Easy
3	Direct link cancellation	Knowing the direct link	Very Strong	Extremely difficult

## V. THE ANALYSIS OF ATTACK EFFECTS

To evaluate the effect of the RIS jamming attack on CRKG, we formulate the secret key rate and then discuss effective regions of RIS deployment.

### A. The Secret Key Rate

In general, the number of secure bits yielded by CRKG is the mutual information between  $\tilde{h}_{ab}$  and  $\tilde{h}_{ba}$  on the condition of  $\tilde{h}_e$  that can be expressed as [2]

$$R = I(\tilde{h}_{ab}; \tilde{h}_{ba} | \tilde{h}_{ae}, \tilde{h}_{be}), \quad (18)$$

where  $\tilde{h}_{ae}$  and  $\tilde{h}_{be}$  are the channels observed by Eve. As  $\tilde{h}_{ae}$  and  $\tilde{h}_{be}$  are assumed to be independent of those of Alice and Bob, the secret key rate degrades to

$$R = I(\tilde{h}_{ab}; \tilde{h}_{ba}) = \log \frac{K_{ab}K_{ba}}{\det(\mathbf{K}_{ab})}, \quad (19)$$

where  $K_{ab}$  and  $K_{ba}$  are respectively covariances of  $\tilde{h}_{ab}$  and  $\tilde{h}_{ba}$ , and  $\mathbf{K}_{ab}$  is the total correlation matrix which is given by

$$\mathbf{K}_{ab} = \mathbb{E} \begin{bmatrix} \tilde{h}_{ab}\tilde{h}_{ab}^* & \tilde{h}_{ab}\tilde{h}_{ba}^* \\ \tilde{h}_{ba}\tilde{h}_{ab}^* & \tilde{h}_{ba}\tilde{h}_{ba}^* \end{bmatrix}. \quad (20)$$

For convenience of calculations, we omit  $t_1$  and  $t_2$  and simplify channel estimates of (14) into

$$\begin{aligned} \tilde{h}_{ab}(k) &= \mathbf{h}_{ar}^T \mathbf{\Lambda} \mathbf{h}_{rb} e^{-j2\pi\tau_r k/K} + h_d(k) + z_b(k), \\ \tilde{h}_{ba}(k) &= \mathbf{h}_{rb}^T \mathbf{\Lambda}' \mathbf{h}_{ar} e^{-j2\pi\tau_r k/K} + h_d(k) + z_a(k). \end{aligned} \quad (21)$$

Then,  $K_{ab}$  and  $K_{ba}$  are calculated as

$$\begin{aligned} K_{ab} &= \mathbb{E}\{\tilde{h}_{ab}\tilde{h}_{ab}^*\} \\ &= \mathbb{E}\{|\mathbf{h}_{ar}^T \mathbf{\Lambda} \mathbf{h}_{rb}|^2 + h_d h_d^* + \sigma^2\} \\ &= \beta_r + \sum_{l=1}^L \beta_l + \sigma^2, \end{aligned} \quad (22)$$

and

$$\begin{aligned} K_{ba} &= \mathbb{E}\{\tilde{h}_{ba}\tilde{h}_{ba}^*\} \\ &= \mathbb{E}\{|\mathbf{h}_{rb}^T \mathbf{\Lambda}' \mathbf{h}_{ar}|^2 + h_d h_d^* + \sigma^2\} \\ &= \beta_{r'} + \sum_{l=1}^L \beta_l + \sigma^2, \end{aligned} \quad (23)$$

respectively.

The cross-terms satisfy  $\mathbb{E}\{\tilde{h}_{ab}\tilde{h}_{ab}^*\} = \mathbb{E}\{\tilde{h}_{ab}\tilde{h}_{ba}^*\} = K_c$ , which is calculated as

$$\begin{aligned} K_c &= \mathbb{E}\{\mathbf{h}_{ar}^T \mathbf{\Lambda} \mathbf{h}_{rb} (\mathbf{h}_{rb}^T \mathbf{\Lambda}' \mathbf{h}_{ar})^* + h_d h_d^*\} \\ &= \beta_{r,r'} + \sum_{l=1}^L \beta_l, \end{aligned} \quad (24)$$

where  $\beta_{r,r'} = \mathbb{E}\{\mathbf{h}_{ar}^T \mathbf{\Lambda} \mathbf{h}_{rb} (\mathbf{h}_{rb}^T \mathbf{\Lambda}' \mathbf{h}_{ar})^*\}$  represents the cross-covariance of the RIS-induced link. Then, the determinant of  $\mathbf{K}_{ab}$  can be calculated as

$$\begin{aligned} \det(\mathbf{K}_{ab}) &= (\beta_r + \sum_{l=1}^L \beta_l + \sigma^2)(\beta_{r'} + \sum_{l=1}^L \beta_l + \sigma^2) \\ &\quad - (\sum_{l=1}^L \beta_l + \beta_{r,r'})^2. \end{aligned} \quad (25)$$

Hence, the secret key rate can be expressed as

$$\begin{aligned} R &= \log \left( \beta_r + \sum_{l=1}^L \beta_l + \sigma^2 \right) + \log \left( \beta_{r'} + \sum_{l=1}^L \beta_l + \sigma^2 \right) \\ &\quad - \log \left( (\beta_r + \sum_{l=1}^L \beta_l + \sigma^2)(\beta_{r'} + \sum_{l=1}^L \beta_l + \sigma^2) \right. \\ &\quad \left. - (\beta_{r,r'} + \sum_{l=1}^L \beta_l)^2 \right). \end{aligned} \quad (26)$$

### B. Case Studies

Next, according to (26), we derive secret key rates of some specific cases to illustrate the effect of the RIS on CRKG:

- *No RIS is deployed:* In the absence of an RIS,  $\beta_{r,r'} = \beta_{r'} = \beta_r = 0$ , and then the secret key rate is given by

$$R_0 = \log \left( 1 + \frac{(\sum_{l=1}^L \beta_l)^2}{\sigma^4 + 2\sigma^2(\sum_{l=1}^L \beta_l)} \right), \quad (27)$$

which serves as a baseline for this paper. For the sake of analysis, we assume that  $\sum_{l=1}^L \beta_l$  is fixed and discuss the change of secret key rates with  $\beta_r$  and  $\sigma^2$ .

- *RIS is not malicious:* Next, we consider the case that an RIS exists, but it is not controlled by Eve. The reflection coefficients of RIS are assumed to be constant during one channel probing period, i.e.,  $\mathbf{\Lambda}' = \mathbf{\Lambda}$ , so  $\beta_{r,r'} = \beta_{r'} = \beta_r$ , and the secret key rate becomes

$$R_1 = \log \left( 1 + \frac{(\beta_r + \sum_{l=1}^L \beta_l)^2}{\sigma^4 + 2\sigma^2(\beta_r + \sum_{l=1}^L \beta_l)} \right). \quad (28)$$

As the power gain of the RIS path,  $\beta_r$ , is positive and the basic function

$$f(x) = \frac{x^2}{a + bx}, \quad a > 0, b > 0, x > 0 \quad (29)$$

increases monotonously along with  $x$ , we obtain that  $R_1 > R_0$ , which indicates that instead of decreasing, an RIS will even increase the secret key rate as long as the change of the RIS path is synchronized with those of physical paths.

- *RIS Jamming Attacks:* Now, we study the secret key rate under RIS jamming attacks. First, we consider that Eve

exploits the asymmetry of RIS structures, i.e.,  $\Lambda' = 0$ , so  $\beta_{r,r'} = \beta_{r'} = 0$  and the secret key rate is derived as

$$R_2 = \log \left( 1 + \frac{(\sum_{l=1}^L \beta_\ell)^2}{\sigma^4 + 2\sigma^2 \sum_{l=1}^L \beta_\ell + \beta_r \sum_{l=1}^L \beta_\ell + \beta_r \sigma^2} \right). \quad (30)$$

Comparing (30) and (27), it is observed that  $R_2$  is smaller than  $R_0$ , since the additional term  $\beta_r \sum_{l=1}^L \beta_\ell + \beta_r \sigma^2$  in the denominator of (30) is positive. When the SNR is high, the gap between  $R_0$  and  $R_2$  is approximately

$$\begin{aligned} \Delta_1 &= R_0 - R_2 \\ &\approx \log \left( \frac{(\sum_{l=1}^L \beta_\ell)^2}{\sigma^4 + 2\sigma^2 \sum_{l=1}^L \beta_\ell} \right) \\ &\quad - \log \left( 1 + \frac{\sum_{l=1}^L \beta_\ell}{\beta_r} \right) \\ &\approx \log \left( \frac{\sum_{l=1}^L \beta_\ell}{2\sigma^2} \frac{\beta_r}{\beta_r + \sum_{l=1}^L \beta_\ell} \right). \end{aligned} \quad (31)$$

Therefore, this gap can be enlarged by increasing  $\beta_r$  or by decreasing  $\sigma^2$ .

Next, we consider another RIS jamming attack, where Eve uses asynchronous RIS configurations. In this case,  $\Lambda'$  is independent of  $\Lambda$  and they have the same covariance, so that  $\beta_{r,r'} = 0$ ,  $\beta_{r'} = \beta_r$  and the secret key rate becomes

$$R_3 = \log \left( 1 + \frac{(\sum_{l=1}^L \beta_\ell)^2}{(\beta_r + \sigma^2)^2 + 2(\beta_r + \sigma^2)(\sum_{l=1}^L \beta_\ell)} \right). \quad (32)$$

Similarly, we find that  $R_3$  is smaller than  $R_0$ , since the additional term  $2\beta_r \sum_{l=1}^L \beta_\ell + 2\beta_r \sigma^2 + \beta_r^2$  in the denominator of (32) is positive. In addition,  $R_3$  is also smaller than  $R_2$ , as  $2\beta_r \sum_{l=1}^L \beta_\ell + 2\beta_r \sigma^2 + \beta_r^2 > \beta_r \sum_{l=1}^L \beta_\ell + \beta_r \sigma^2$ , which indicates that as an RIS jamming attack, asynchronous RIS configurations works better than asymmetric RIS structures.

Define  $\Delta_2 = R_0 - R_3$  as the gap between this case and the baseline, and let  $\Delta_3 = R_2 - R_3$  denote the gap between the two RIS jamming attacks. At high SNR, these values are approximated by

$$\begin{aligned} \Delta_2 &\approx \log \left( \frac{(\sum_{l=1}^L \beta_\ell)^2}{\sigma^4 + 2\sigma^2(\sum_{l=1}^L \beta_\ell)} \right) \\ &\quad - \log \left( 1 + \frac{(\sum_{l=1}^L \beta_\ell)^2}{\beta_r^2 + 2\beta_r(\sum_{l=1}^L \beta_\ell)} \right) \\ &\approx \log \left( \frac{(\sum_{l=1}^L \beta_\ell)\beta_r}{2\sigma^2} \frac{\beta_r + 2(\sum_{l=1}^L \beta_\ell)}{(\beta_r + \sum_{l=1}^L \beta_\ell)^2} \right), \end{aligned} \quad (33)$$

and

$$\begin{aligned} \Delta_3 &\approx \log \left( 1 + \frac{\sum_{l=1}^L \beta_\ell}{\beta_r} \right) - \log \left( 1 + \frac{(\sum_{l=1}^L \beta_\ell)^2}{\beta_r^2 + 2\beta_r(\sum_{l=1}^L \beta_\ell)} \right) \\ &= \log \left( 1 + \frac{\sum_{l=1}^L \beta_\ell}{\beta_r + \sum_{l=1}^L \beta_\ell} \right) \\ &= \log \left( 1 + \frac{1}{1 + \frac{\beta_r}{\sum_{l=1}^L \beta_\ell}} \right), \end{aligned} \quad (34)$$

respectively. As observed,  $\Delta_2$  increases with the decline of  $\sigma^2$ . It also rises with the increase of  $\beta_r$  and it tends to be constant in the end. Conversely,  $\Delta_3$  only decreases with the power of the RIS path  $\beta_r$ .

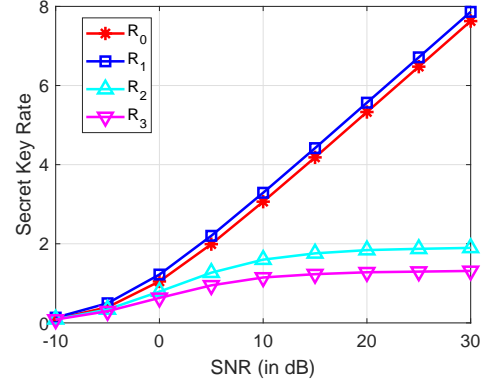


Fig. 3: Different secret key rates versus SNR ( $\beta = 1$ ).

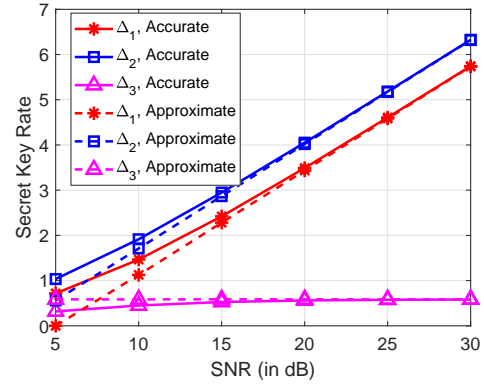


Fig. 4: The differences between different secret key rates versus different SNR ( $\beta = 1$ ).

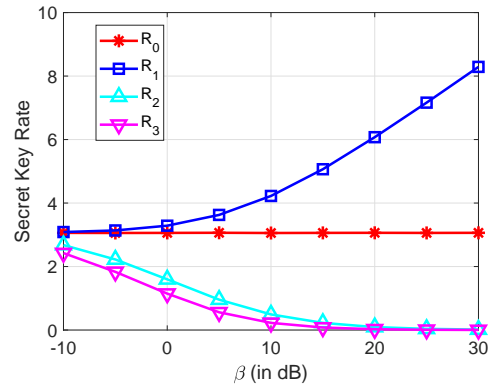


Fig. 5: Different secret key rates versus  $\beta$  (SNR = 10 dB).

Next, we use Monte Carlo simulations to present numerical results of secret key rates to verify the above theoretical analysis. Without loss of generality, we assume that the number of paths is  $L = 4$ . The distance of each path is generated

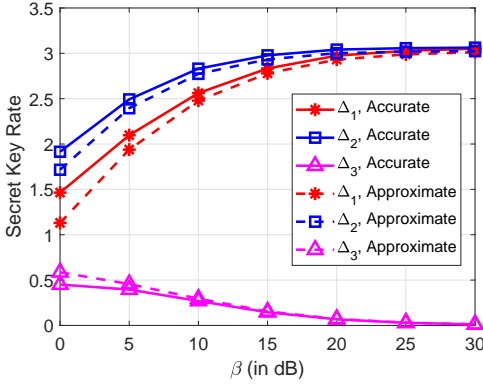


Fig. 6: The differences between different secret key rates versus  $\beta$  (SNR = 10 dB).

according to the uniform distribution of the scatter in a range of  $10 \text{ m} \times 10 \text{ m}$ . Following [30], in the simulation, the dielectric substrate of the meta-atom in the RIS is assumed to be RO4003 with relative permittivity of 3.55. Figure 3 reports the secret key rates, including  $R_0$ ,  $R_1$ ,  $R_2$ , and  $R_3$ , as functions of the SNR, which is equal to  $1/\sigma^2$ . The RIS power is set as  $\beta = 1$ . It is observed that  $R_0$  and  $R_1$  are significantly higher than  $R_2$  and  $R_3$ , which is in agreement with the previous theoretical analysis that RIS jamming attacks can reduce the secret key rate. Although all curves grow with SNR, the curves of  $R_0$  and  $R_1$  have almost linear increases, while the curves of  $R_2$  and  $R_3$  become less steep when the SNR is larger than 20 dB. Specifically,  $R_1$  is slightly larger than  $R_0$  as a harmless RIS would provide an additional channel path for key generation. Regarding RIS jamming attacks,  $R_3$  is one-fourth lower than  $R_2$  since asynchronous RIS configuration would affect both forward and backward RIS-induced channels while the asymmetry of RIS structure only has an impact on one direction. Figure 4 further demonstrates the differences between these secret key rates, including accurate values and approximate values as given in (31), (33) and (34). These approximate values are proved to be good as they are very close to accurate values at high SNR.  $\Delta_1$  and  $\Delta_2$ , representing the rate decrease caused by the above two RIS jamming attacks, rise almost linearly with SNR, while their difference, i.e.,  $\Delta_3$ , is basically fixed over SNR. These curves are consistent with the theoretical analysis of  $\Delta_1$ ,  $\Delta_2$ , and  $\Delta_3$ .

In Fig. 5, we compare the secret key rates for SNR = 10 dB as a function of the RIS units power  $\beta$ , which can be enlarged by adding a power amplifier. The power of RIS path  $\beta_r$  increases with  $\beta$  linearly. The original secret key rate  $R_0$  without RIS is not affected by  $\beta$ , while  $R_1$  rises with  $\beta$  due to the power increase of the additional channel path provided by a harmless RIS. Conversely, if RIS is malicious, the secret key rates  $R_2$  and  $R_3$  drop with the growth of  $\beta$  rapidly, approaching close to zero when  $\beta$  surpasses 10 dB. The curve of  $R_3$  falls even faster than that of  $R_2$ . The result in Fig. 5 substantiates the statement that the negative effect of RIS jamming attacks on the secret key rate can be enhanced by increasing  $\beta$ . Figure 6 further compares the differences of secret key rates as a function of  $\beta$ . The approximate values

of  $\Delta_1$ ,  $\Delta_2$ , and  $\Delta_3$  are close to their corresponding accurate values, especially when  $\beta$  is larger than 10 dB. The curves of  $\Delta_1$  and  $\Delta_2$  increase with  $\beta$ , while the curve of  $\Delta_3$  decreases with  $\beta$ . All curves become gradually flattened at  $\beta = 20$  dB. This is caused by the fact that secret key rates under two RIS jamming attacks are both close to zero at high  $\beta$ .

From the above discussion, we have found that RIS jamming attacks can reduce the secret key rate and their negative effects will be enhanced by increasing the power gain of the RIS path.

### C. The Effective Region for RIS Deployment

Recall that the power gain of the RIS path  $\beta_r = \beta |\Gamma \cos(\theta)|^2 / d_r^2$ , in addition to  $\beta$ ,  $\beta_r$  also varies with position. Therefore, from the Eve's point of view, she should choose an appropriate position of RIS to enhance its attack effects.

According to (6) and (7), the channel gain of the RIS path is

$$\beta_r = \beta \frac{\cos^2 \theta}{d_r^2} \left| \frac{\epsilon_r \cos \theta - \sqrt{\epsilon_r - \sin^2 \theta}}{\epsilon_r \cos \theta + \sqrt{\epsilon_r - \sin^2 \theta}} \right|^2, \quad (35)$$

which depends on its propagation distance  $d_r$  and incident angle  $\theta$ . The further the distance, the greater the attenuation. Generally, the bigger the angle, the smaller the reflectivity. Therefore, if Eve would like to increase  $\beta_r$ , the RIS should be placed at a position where the RIS-path has a small propagation distance and a small incident angle.

To find more insights on RIS positions, we further express  $\beta_r$  as a function of  $d_{ar}$  and  $H$ . As shown in Fig. 1,  $d_r$  is the sum of the distance between Alice and RIS and that between RIS and Bob, i.e.,

$$d_r = \sqrt{d_{ar}^2 + H^2} + \sqrt{(D - d_{ar})^2 + H^2}. \quad (36)$$

The double angle  $2\theta$  satisfies the Cosine law that

$$\begin{aligned} \cos 2\theta &= \frac{(d_{ar}^2 + H^2) + [(D - d_{ar})^2 + H^2] - D^2}{2 \cdot \sqrt{d_{ar}^2 + H^2} \cdot \sqrt{(D - d_{ar})^2 + H^2}}, \quad (37) \\ &= \frac{d_{ar}^2 + H^2 - d_{ar}D}{\sqrt{d_{ar}^2 + H^2} \cdot \sqrt{(D - d_{ar})^2 + H^2}}. \end{aligned}$$

Therefore, the incident angle  $\theta$  is given by

$$\theta = \frac{1}{2} \cdot \arccos \frac{d_{ar}^2 + H^2 - d_{ar}D}{\sqrt{d_{ar}^2 + H^2} \cdot \sqrt{(D - d_{ar})^2 + H^2}}. \quad (38)$$

Substituting (36) and (38) into (35),  $\beta_r$  can be expressed as a function of  $H$  and  $d_{ar}$ . This function, however, is complicated, making it difficult to find a closed-form expression of effective  $(d_{ar}, H)$ . As a result, we give some numerical results as follows. Fig. 7 shows the energy gain of RIS path for different positions of RIS, which is calculated according to (35). As observed,  $\beta_r$  is significantly larger than others, when it is placed near Alice/Bob. It is because in this case,  $\theta$  approaches zero and  $d_r$  is close to  $D$ , guaranteeing a high reflectivity and a small attenuation, respectively. Nonetheless, to avoid detection, the RIS should still not be placed too close to Alice/Bob. From the numerical results,  $\beta_r$  is still larger than



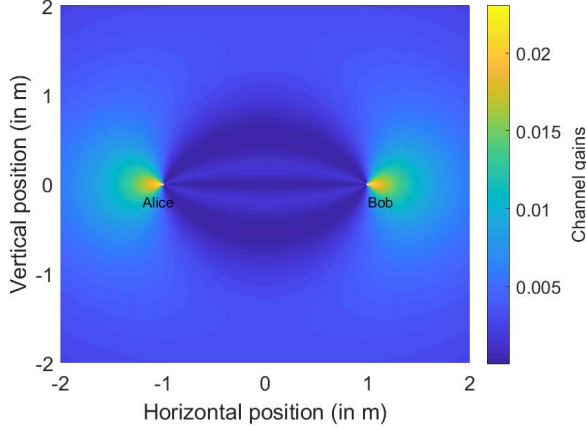


Fig. 7: RIS channel gains at different positions.

0.01, when the distance between Alice/Bob and RIS is 20% of that between Alice and Bob. In other words, it is feasible for Eve to perform RIS jamming attacks in these regions.

## VI. CPR-CRKG: A COUNTERMEASURE IN WIDEBAND OFDM SYSTEMS

This section introduces a countermeasure to resist the previously described RIS jamming attacks and demonstrates its effectiveness through numerical simulations.

### A. Protocol Description

Generally, an RIS jamming attack is challenging to prevent. The key reason for this is the entirely passive operation of the RIS, making the RIS jamming attack almost imperceptible. Further, in view of RIS jamming, traditional anti-jamming techniques such as fast frequency hopping should be considered ineffective. That is, the RIS reflects and alters the legitimate signals regardless of their frequency (assuming a sufficiently large RIS operation bandwidth).

From the previous study of the secret key rate, we have found that although Eve decreases the similarity of channel frequency responses over all subcarriers, only the RIS-induced path is affected. If the contaminated path can be distinguished from others, Alice and Bob are still able to generate secret keys from the remaining uncontaminated paths. Following this intuition, we propose a new secret key generation protocol based on contaminated path removal, referred to as CPR-CRKG. Its main task is to resist the above RIS jamming attacks while still being able to generate a matching key material. Fig. 8 depicts the block diagram of CPR-CRKG and its protocol is elaborated in the following.

- 1) Like in a conventional CRKG procedure, Alice and Bob alternately transmit pilot signals to each other. During each channel coherence time,  $N_p$  pairs of channel estimates, i.e.,

$$\begin{aligned} \tilde{\mathbf{H}}_{ba} &= [\tilde{\mathbf{h}}_{ba}^1, \tilde{\mathbf{h}}_{ba}^2, \dots, \tilde{\mathbf{h}}_{ba}^{N_p}], \\ \tilde{\mathbf{H}}_{ab} &= [\tilde{\mathbf{h}}_{ab}^1, \tilde{\mathbf{h}}_{ab}^2, \dots, \tilde{\mathbf{h}}_{ab}^{N_p}], \end{aligned} \quad (39)$$

are collected by Alice and Bob, respectively.

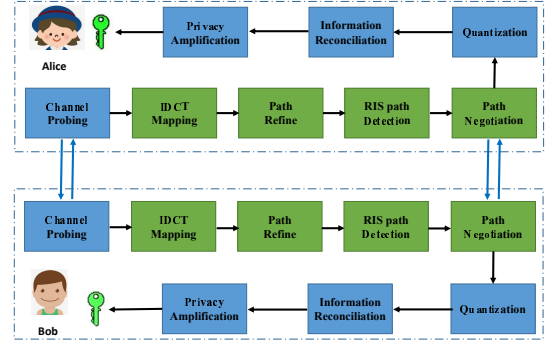


Fig. 8: Block diagram of the proposed CPR-CRKG method.

- 2) Taking advantage of the wideband OFDM system, Alice and Bob perform an Inverse Discrete Cosine Transformation (IDCT) to map  $\tilde{\mathbf{H}}_{ba}$  and  $\tilde{\mathbf{H}}_{ab}$  into the time-domain, which are obtained by

$$\tilde{\mathbf{G}}_{ba} = \mathbf{F}\tilde{\mathbf{H}}_{ba}, \tilde{\mathbf{G}}_{ab} = \mathbf{F}\tilde{\mathbf{H}}_{ab}, \quad (40)$$

where the transformation matrix  $\mathbf{F} \in \mathbb{C}^{K \times K}$  is given by

$$\mathbf{F} = \begin{bmatrix} 1 & 1 & \dots & 1 \\ e^{j2\pi/K} & e^{j4\pi/K} & \dots & e^{j2K\pi/K} \\ e^{j4\pi/K} & e^{j8\pi/K} & \dots & e^{j4K\pi/K} \\ \vdots & \vdots & \ddots & \vdots \\ e^{j2K\pi/K} & e^{j4K\pi/K} & \dots & e^{j2K^2\pi/K} \end{bmatrix}. \quad (41)$$

Rows and columns of the transformed matrices, including  $\tilde{\mathbf{G}}_{ba}$  and  $\tilde{\mathbf{G}}_{ab}$ , represent relative time delays and channel probing rounds, respectively.

- 3) Since the number of channel paths is far less than  $K$ ,  $\tilde{\mathbf{G}}_{ba}$  and  $\tilde{\mathbf{G}}_{ab}$  are both sparse matrices that should be refined. For each column of them, the top  $N_{sel}$  rows with the highest power gain are regarded as significant paths at a certain channel probing round. To facilitate understanding, we use  $d_{k,n} = 1$  to present  $\tilde{g}(k,n)$  as a significant path at a relative time delay  $k$  and channel probing round  $n$ , otherwise  $d_{k,n} = 0$ . To avoid accidental error, row  $k$  is recorded in a set  $\mathbb{K}_A/\mathbb{K}_B$  by Alice/Bob only when it is recognized as significant paths for no less than  $\alpha$  times among all  $N_p$  columns, i.e.,  $\sum_{n=1}^{N_p} d_{k,n} \geq \alpha$ .
- 4) Alice and Bob detect whether a potential RIS path exists in their significant path set. Recalling that for the RIS jamming attack based on the asynchronism of RIS configurations, Eve needs to increase the switching frequency of the RIS to introduce a considerable temporal deviation. In this case, the channel gain of the RIS-induced path would change more quickly than other paths. Following this idea, we use the autocorrelation coefficients of paths for detection. For each path  $k \in \mathbb{K}_A/\mathbb{K}_B$ , Alice and Bob calculate its autocorrelation function as

$$R(j) = \sum_{n=1}^{N_p} \tilde{g}(k, n+j)\tilde{g}^*(k, n), \quad (42)$$

where  $j$  is the offset of the channel probing round. If one path has a significantly more rapidly descending

autocorrelation function than others in the set, this path is recognized as an RIS-induced path. Alice and Bob drop their recognized RIS-induced paths from  $\mathbb{K}_A$  and  $\mathbb{K}_B$ , respectively, and would thus mitigate the effect of a potential RIS jamming attack.

- 5) Alice and Bob negotiate a group of available channel paths by exchanging  $\mathbb{K}_A$  and  $\mathbb{K}_B$ . The intersection set  $\mathbb{K} = \mathbb{K}_A \cap \mathbb{K}_B$  is selected as the group of negotiated available channel paths. For the RIS jamming attack based on the asymmetry of RIS structures, the RIS-induced path only may appear in  $\mathbb{K}_B$  and thus would not be selected as an available channel path. Therefore, the negative effect of this RIS jamming attack is also avoided. Alice and Bob average those channel gains of paths in  $\mathbb{K}$  on the column and obtain

$$\begin{aligned} \tilde{g}_{ab} &= [\tilde{g}_{ab}(1), \tilde{g}_{ab}(2), \dots, \tilde{g}_{ab}(K_e)]^T, \\ \tilde{g}_{ba} &= [\tilde{g}_{ba}(1), \tilde{g}_{ba}(2), \dots, \tilde{g}_{ba}(K_e)]^T, \end{aligned} \quad (43)$$

where  $K_e$  is the number of paths in  $\mathbb{K}$  and the averaged value on the  $k$ -th path is given by  $\tilde{g}_{ab}(k) = \frac{1}{N_p} \sum_{n=1}^{N_p} h_{ab}^n(k)$ .

- 6) Alice and Bob collect  $\tilde{g}_{ab}$  and  $\tilde{g}_{ba}$  over multiple channel coherence times and quantize the gain of each channel path using single-bit CDF quantization [24]. These quantized bit strings, denoted by  $\mathbf{k}_A$  and  $\mathbf{k}_B$ , are also referred to as raw secret keys, which can be converted into secret keys through information reconciliation and privacy amplification. As these steps are similar to those used in existing key generation schemes, we do not pay particular attention to them and focus our attention only on mitigating RIS jamming attacks and improving the similarity between  $\mathbf{k}_A$  and  $\mathbf{k}_B$ .

As outlined above, CPR-CRKG wipes out the contaminated path and therefore removes the effect of the RIS from the channel, effectively mitigating the effect of both asymmetric RIS structures and asynchronous RIS configurations.

### B. Numerical simulation

We demonstrate the negative effects of RIS jamming attacks and verify the effectiveness of CPR-CRKG in a wideband OFDM system with the aid of numerical simulations. The system bandwidth is set as 100 MHz and other simulation settings remain the same as that given in Section V-B.

Figure 9 reports the BDR of raw secret keys as a function of SNR. The BDR is defined as the ratio between the number of disagreement bits and the number of total bits. Generally, all BDR curves drop with SNR. The difference is that the BDR of the original scheme is close to zero at high SNR, while the last four schemes have an error floor. Specifically, without the RIS jamming attack, the BDR of the original CRKG scheme is lower than 0.1, when SNR surpasses 10 dB. Under RIS jamming attacks, the BDR curves fall and reach an error floor of 0.15 and 0.2, respectively. The RIS jamming attack based on the asymmetry of RIS structures (Attack 1) has a lower BDR than that based on the asynchronism of RIS configurations (Attack 2), which is in agreement with the theoretical analysis in Section V. The dashed curves of BDR

are roughly one-fourth that of their corresponding solid curves, demonstrating the effectiveness of the proposed CPR-CRKG scheme. Notably, the BDRs of CPR-CRKG also have error floors, which is caused by the fact that the system bandwidth is limited, so the non-reciprocity caused by the RIS-induced path would also affect other paths after the IDCT mapping step of CPR-CRKG. As attack 2 causes more severe non-reciprocity than attack 1, the BDR of CPR-CRKG under attack 2 is slightly higher than that under attack 1.

Figure 10 shows the BDRs of different schemes as a function of  $\beta$ . Except for the original CRKG scheme, the BDR of all other considered schemes rises with  $\beta$  rapidly, which is consistent with the results in Fig. 5. It is also observed that the gaps between CRKG under attack and our CPR-CRKG scheme are enlarged when  $\beta$  increases from 0 dB to 20 dB. This is because when  $\beta$  is large, the RIS-induced path becomes more evident and is thus easier to detect. The results in Fig. 9 and Fig. 10 substantiate the statement that RIS jamming attacks have a non-negligible negative effect on the BDR. Further, our results confirm that the proposed CPR-CRKG scheme can mitigate the effect of the RIS jamming attack.

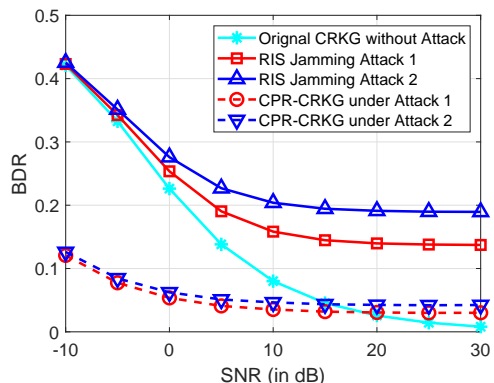


Fig. 9: The BDR of different CRKG schemes versus SNR ( $\beta = 1$ ).

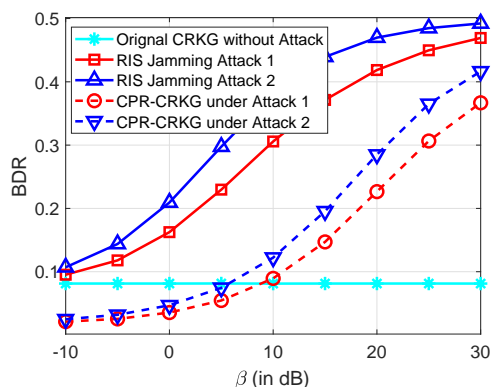


Fig. 10: The BDR of different CRKG schemes versus  $\beta$  (SNR = 10 dB).

## VII. EXPERIMENTAL RESULTS

In this section, we present the results of experimental investigations of the RIS jamming attack based on the asynchronism of RIS configurations and its countermeasure.

### A. Experimental Setup

In our experiments, we place the parties Alice, Bob, and Eve within line-of-sight in an indoor environment. The legitimate parties Alice and Bob perform a CRKG procedure with the goal of establishing a common encryption key. The passive attacker Eve pursues the goal of disrupting the CRKG procedure with an RIS. We now outline additional details of key elements of the setup.

**Alice and Bob.** We utilize commodity Wi-Fi devices based on ath9k network interface cards (NICs) for IEEE 802.11n Wi-Fi in a 2x2 MIMO configuration. The parties transmit at approx. 5 dBm on Wi-Fi channel 60 at 5.3 GHz with 40 MHz bandwidth. For each received packet and spatial MIMO channel, both parties obtain a complex vector containing the CSI data for each of the 114 non-zero OFDM subcarriers [31].

In our experiments, Alice and Bob exchange Wi-Fi packets in a ping-pong manner to perform bidirectional channel probing, see right side of Figure. 11. The channel probing rate  $f_p$  is adjustable by delaying the pong response packets by  $T_p = \frac{1}{f_p}$  (relative to the reception of ping packets). The time series of channel measurements are translated to bit strings using single-bit CDF quantization [24]. To assess the CRKG performance, we utilize average BDR over all OFDM subcarrier and spatial channels.

**Eve.** We use a prototype RIS with 256 unit-cell elements arranged in a  $16 \times 16$  array on an FR4 PCB measuring  $43 \times 35$  cm. Each rectangular unit cell reflector utilizes a PIN diode to achieve 1-bit phase control, i.e., an impinging wave is either reflected with phase shift 0 or  $\pi$ . The RIS prototype is designed to realize this behavior at around 5.35 GHz. An onboard microcontroller controls the unit cells by means of cascaded shift registers. The RIS prototype is an evolution of our design from [32], where we used a higher-cost substrate and a smaller array size. Following Section IV, in our experiments we apply random RIS configurations with an update period  $T_r = \frac{1}{f_r}$ , see right side of Figure. 11.

**Environment.** We conduct the experiment in an ordinary indoor environment at our institute building. Since this room does not exhibit sufficient variation for CRKG, we introduce randomness by means of a random scatterer. It consists of a rod holding thin stripes of aluminum foil which move randomly due to airflow from a cooling fan.

### B. Timing Aspects

For RIS jamming, the attacker aims to disrupt the CRKG channel probing phase by changing the RIS configuration during the bidirectional measurement of the channel. Thus, the attack performance depends on the speed of the adversarial RIS and the legitimate channel probing. To assess this experimentally, we place the parties as shown in Figure 11. For various RIS updating and channel probing rates, we

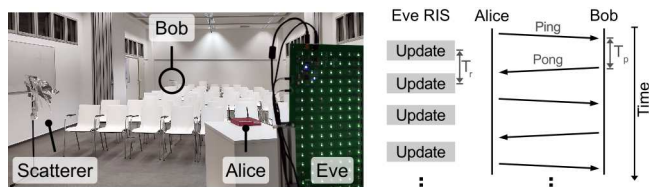


Fig. 11: Left: Experimental setup in a seminar room. Right: Illustration of the CRKG channel probing timing and the attacker's concurrent RIS operation.

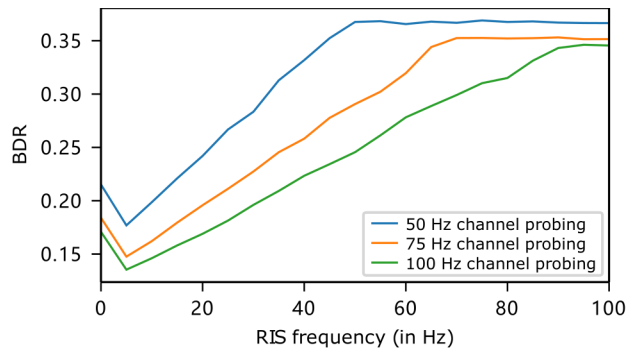


Fig. 12: BDR of Alice and Bob over RIS modulation speed.

take 500 bidirectional channel samples. Figure 12 shows the BDR of Alice and Bob as a function of the RIS modulation frequency for channel probing rates 50, 75, and 100 Hz.

We can see that the BDR increases linearly with the RIS frequency until a plateau is reached when  $f_p = f_r$ . This is expected since the probability of an RIS update taking place between ping and pong packets is  $f_r/f_p$  as long as  $f_r < f_p$  (assuming the RIS reconfiguration and packet duration times to be negligible). Further, we can see that the BDR without an attack at  $f_p = 0$  reduces with the channel probing rate as effects from non-simultaneous channel probing are minimized. Interestingly, for low RIS frequencies such as  $f_r \approx 5$  Hz, the BDR is reduced since the RIS modulation contributes more to the channel variation than corrupting channel reciprocity.

Our experiment shows that RIS jamming attacks are feasible in practice by rapidly applying random configurations to the RIS. The attack is of low complexity as the attacker operates independently and asynchronously from the legitimate CRKG process. However, to reach maximum attack efficiency, the RIS modulation speed should be chosen at least as high as the legitimate channel probing speed.

### C. Attacker Position

Next, we investigate how the RIS position affects the attack's effectiveness. From Section V-C, we expect the ideal RIS position for successful RIS jamming to be in proximity to the legitimate parties with a small incident angle.

In the experiment, we place the RIS at 27 different positions facing towards Alice. The positions (see Figure 13) were chosen to cover a number of combinations of distances and incident angles. For each position, the RIS first remains constant and then is modulated at 100 Hz update frequency.

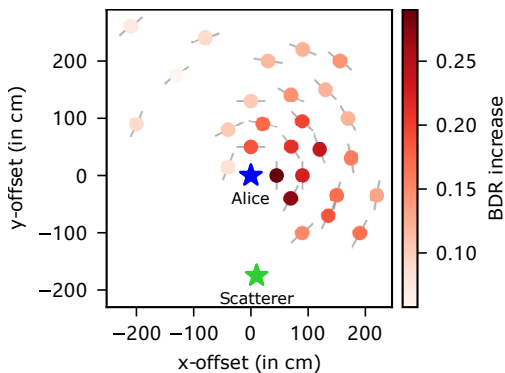


Fig. 13: Positions of the attacker RIS. The color scheme indicates the BDR increase due to the RIS jamming attack. The grey lines indicate the RIS orientation (facing towards Alice). Bob is located at  $(-1240 \text{ cm}, -275 \text{ cm})$ .

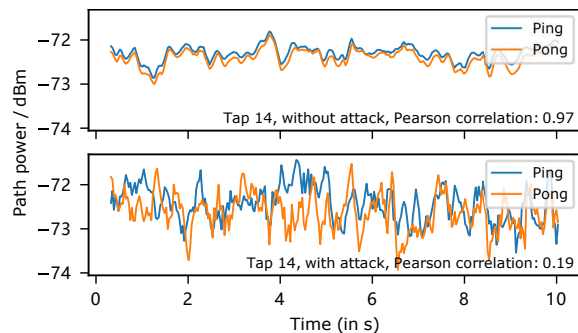
For both cases, the legitimate parties perform channel probing at 100 Hz to collect 5000 bidirectional channel samples.

We quantify the attack effectiveness using the BDR increase between the cases with modulated and constant RIS. Figure 13 shows the BDR increase for each RIS position. We can clearly observe that the attack works best when the attacker is rather close to Alice with a small incident angle which is consistent with the theoretical results. In our experiment, the RIS was capable of increasing the BDR by up to approx. 30% in close proximity to Alice. While such positions may be considered impractical to launch an attack, we still observed reasonable attack performance with BDR increases of around 20% at positions with approx. 2 m distance. Despite that, active RIS implementations, e.g., [33], which are equipped with power amplifiers could be utilized to overcome distance limitations.

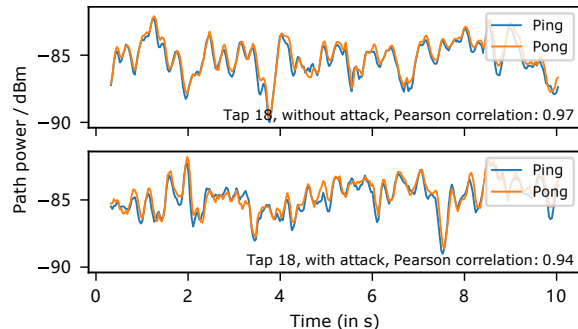
#### D. Path Separation

Next, to assess the feasibility of the CPR-CRKG scheme described in Section VI, we experimentally evaluate path separation in the time domain as a countermeasure against RIS jamming. To obtain the accurate power delay profile (PDP) from Wi-Fi CSI data, additional processing is necessary [31] to address phase imperfections. Therefore, to simplify the study and solely focus on the proposed countermeasure, we employ a Keysight P9372A vector network analyzer (VNA) for channel probing. Other than this, the experimental setup remains as outlined before. We connect the VNA via coaxial cables to one antenna of each party and measure the complex scattering parameters  $S_{21}(f)$  and  $S_{12}(f)$ . These represent the forward and reverse transmission measured by Alice and Bob, respectively. We measure over an 80 MHz bandwidth to achieve a spatial resolution comparable with typical Wi-Fi and take 80 points for each measurement which yields a VNA sweep time of approx. 16 ms.

For the experiment, we place the RIS in approx. 1 m distance to Alice. We position the random scatterer such that the difference in path lengths between the RIS and the scatterer is greater than the spatial resolution of approx. 3.75 m. We then perform channel probing with and without the RIS being randomly configured over time. Using the inverse Fourier



(a) Power over time, 14<sup>th</sup> PDP tap.



(b) Power over time, 18<sup>th</sup> PDP tap.

Fig. 14: PDP taps with (upper) and without (bottom) attack.

transform, we obtain the PDP from the frequency domain measurements. As outlined in Section VI, it is possible to separate RIS-affected channel paths in the delay domain. To demonstrate the underlying principle, we plot the magnitudes of the 14<sup>th</sup> and 18<sup>th</sup> PDP taps with and without attack in Figure 14. The propagation paths via the RIS fall into PDP tap 14, causing severe degradation of channel reciprocity as indicated by the Pearson correlation coefficient dropping from 0.97 to 0.19. For PDP tap 18, however, the RIS only has minimal effect and channel reciprocity remains intact. Using the attack detection and the protocol proposed in Section VI, Alice and Bob would drop PDP tap 14 and could use unaffected other paths, such as PDP tap 18, to run the CRKG procedure. Thus, our experiment shows that path separation indeed is a viable countermeasure to tackle RIS jamming in wideband systems as long as the source of randomness and the RIS propagation paths are separable.

## VIII. CONCLUSION

In this paper, we studied CRKG under a new RIS-enabled attack which we coin RIS jamming attack. In the attack, the reciprocal direct link between the legitimate parties is jammed by the RIS-induced link, effectively reducing reciprocity. A general RIS-involved model was built and on that basis, the principle of RIS jamming attack was introduced. We elaborated on three examples of the RIS jamming attack realizations and evaluated them in view of of attack requirements, destructiveness, and implementation. The attack effect was then studied by formulating the secret key rate with a relationship to the deployment of the malicious RIS. Numerical results

verified that RIS jamming attacks can reduce the secret key rate significantly and the reduction rises with the SNR and the RIS unit's power, which were in agreement with the theoretical analysis. Next, we proposed CRP-CRKG as a countermeasure to resist RIS jamming attacks. This countermeasure exploits wideband signals for path separation to distinguish the malicious RIS-induced path, deriving secret keys from the remaining channel path gains. We conducted both simulations and experiments on the RIS jamming attack and CRP-CRKG. The experimental platform consisted of commodity Wi-Fi devices in conjunction with a fabricated RIS prototype. Both simulation and experimental results substantiated the statement that RIS jamming attacks have a non-negligible negative effect on BDR. Moreover, our results show that the proposed CRP-CRKG scheme mitigates the effect of RIS jamming in wideband systems as long as the source of randomness and the RIS propagation paths are separable. Our future work will focus on countermeasures for scenarios where the system bandwidth is not wide enough.

## REFERENCES

- [1] M. Ylianttila, R. Kantola, A. V. Gurtov, and et al., "6G white paper: Research challenges for trust, security and privacy," *CoRR*, vol. abs/2004.11665, 2020. [Online]. Available: <https://arxiv.org/abs/2004.11665>
- [2] U. M. Maurer, "Secret key agreement by public discussion from common information," *IEEE Trans. Inf. Theory*, vol. 39, no. 3, pp. 733–742, 1993.
- [3] S. Mathur, W. Trappe, N. Mandayam, C. Ye, and A. Reznik, "Radio-telepathy: Extracting a secret key from an unauthenticated wireless channel," Phoenix, AZ, USA, Apr. 2008, pp. 128–139.
- [4] G. Li, Z. Zhang, J. Zhang, and A. Hu, "Encrypting wireless communications on the fly using one-time pad and key generation," *IEEE Internet of Things J.*, vol. 8, no. 1, pp. 357–369, 2021.
- [5] J. R. Carson, "A generalization of the reciprocal theorem," *The Bell System Technical Journal*, vol. 3, no. 3, pp. 393–399, 1924.
- [6] W. Tang, X. Chen, M. Z. Chen, J. Y. Dai, Y. Han, S. Jin, Q. Cheng, G. Y. Li, and T. J. Cui, "On channel reciprocity in reconfigurable intelligent surface assisted wireless networks," *IEEE Wireless Commun. Mag.*, vol. 28, no. 6, pp. 94–101, 2021.
- [7] W. Chen, L. Bai, W. Tang, S. Jin, W. X. Jiang, and T. J. Cui, "Angle-dependent phase shifter model for reconfigurable intelligent surfaces: Does the angle-reciprocity hold?" *IEEE Commun. Lett.*, vol. 24, no. 9, pp. 2060–2064, 2020.
- [8] M. Di Renzo, A. Zappone, M. Debbah, M.-S. Alouini, C. Yuen, J. de Rosny, and S. Tret'yakov, "Smart radio environments empowered by reconfigurable intelligent surfaces: How it works, state of research, and the road ahead," *IEEE J. Sel. Areas Commun.*, vol. 38, no. 11, pp. 2450–2525, 2020.
- [9] E. V. Belmega and A. Chorti, "Protecting secret key generation systems against jamming: Energy harvesting and channel hopping approaches," *IEEE Trans. Inf. Forensics Security*, vol. 12, no. 11, pp. 2611–2626, 2017.
- [10] G. Li, L. Hu, P. Staat, H. Elders-Boll, C. Zenger, C. Paar, and A. Hu, "Reconfigurable intelligent surface for physical layer key generation: Constructive or destructive?" *IEEE Wireless Commun. Mag.*, vol. 29, no. 4, pp. 146–153, 2022.
- [11] N. Gao, Y. Han, N. Li, S. Jin, and M. Matthaiou, "When Physical Layer Key Generation Meets RIS: Opportunities, Challenges, and Road Ahead," *arXiv e-prints*, Oct. 2022.
- [12] Z. Ji, P. L. Yeoh, G. Chen, and et al., "Random shifting intelligent reflecting surface for OTP encrypted data transmission," *IEEE Wireless Commun. Lett.*, vol. 10, no. 6, pp. 1192–1196, Feb. 2021.
- [13] Z. Ji, P. L. Yeoh, D. Zhang, and et al., "Secret key generation for intelligent reflecting surface assisted wireless communication networks," *IEEE Trans. Veh. Technol.*, vol. 70, no. 1, pp. 1030–1034, Dec. 2021.
- [14] L. Jin, X. Xu, S. Han, J. Liu, R. Meng, and H. Chen, "Ris-assisted physical layer key generation and transmit power minimization," in *2022 IEEE Wireless Communications and Networking Conference (WCNC)*, 2022, pp. 2065–2070.
- [15] X. Lu, J. Lei, Y. Shi, and W. Li, "Intelligent reflecting surface assisted secret key generation," *IEEE Signal Process. Lett.*, vol. 28, pp. 1036–1040, Feb. 2021.
- [16] Z. Wei, L. Wang, and W. Guo, "Secret key rate upper-bound for reconfigurable intelligent surface-combined system under spoofing," in *IEEE 96th Vehicular Technology Conference (VTC2022-Fall)*, London, United Kingdom, Sept. 2022, pp. 1–6.
- [17] G. Li, C. Sun, W. Xu, M. D. Renzo, and A. Hu, "On maximizing the sum secret key rate for reconfigurable intelligent surface-assisted multiuser systems," *IEEE Trans. Inf. Forensics Security*, vol. 17, pp. 211–225, 2022.
- [18] T. Lu, L. Chen, J. Zhang, K. Cao, and A. Hu, "Reconfigurable intelligent surface assisted secret key generation in quasi-static environments," *IEEE Commun. Lett.*, vol. 26, no. 2, pp. 244–248, 2022.
- [19] L. Jiao, G. Sun, J. Le, and K. Zeng, "Machine learning-assisted wireless PHY key generation with reconfigurable intelligent surfaces," in *Proceedings of the 3rd ACM Workshop on Wireless Security and Machine Learning*, Abu Dhabi, UAE, Jun. 2021, pp. 61–66.
- [20] P. Staat, H. Elders-Boll, M. Heinrichs, R. Kronberger, and et al., "Intelligent reflecting surface-assisted wireless key generation for low-entropy environments," in *Proc. Annual International Symposium on Personal, Indoor and Mobile Radio Communications (PIMRC)*, Virtual, Sept. 2021, pp. 1–7.
- [21] P. Staat, H. Elders-Boll, M. Heinrichs, C. Zenger, and C. Paar, "Mirror, mirror on the wall: Wireless environment reconfiguration attacks based on fast software-controlled surfaces," in *Proceedings of the 2022 ACM on Asia Conference on Computer and Communications Security*, ser. ASIA CCS '22. New York, NY, USA: Association for Computing Machinery, 2022, p. 208–221. [Online]. Available: <https://doi.org/10.1145/3488932.3497767>
- [22] L. Hu, G. Li, H. Luo, and A. Hu, "On the RIS manipulating attack and its countermeasures in physical-layer key generation," in *IEEE 94th Vehicular Technology Conference (VTC2021-Fall)*, Virtual, Sept. 2021, pp. 1–5.
- [23] A. F. Molisch, *Wireless Communications*, 2nd ed. Wiley Publishing, 2011.
- [24] N. Patwari, J. Croft, S. Jana, and S. K. Kasera, "High-rate uncorrelated bit extraction for shared secret key generation from channel measurements," *IEEE Trans. Mobile Comput.*, vol. 9, no. 1, pp. 17–30, 2010.
- [25] C. Zenger, J. Zimmer, J.-F. Pospielek, and C. Paar, "On-line entropy estimation for secure information reconciliation," in *proceedings of the 12th EAI International Conference on Mobile and Ubiquitous Systems: Computing, Networking and Services on 12th EAI International Conference on Mobile and Ubiquitous Systems: Computing, Networking and Services*, 2015, pp. 254–259.
- [26] C. T. Zenger, A. Ambekar, F. Winzer, T. Pöppelmann, H. D. Schotten, and C. Paar, "Preventing scaling of successful attacks: A cross-layer security architecture for resource-constrained platforms," in *Cryptography and Information Security in the Balkans: First International Conference, BalkanCryptSec 2014, Istanbul, Turkey, October 16-17, 2014, Revised Selected Papers 1*. Springer, 2015, pp. 103–120.
- [27] C. T. Zenger, M. Pietersz, and C. Paar, "Preventing relay attacks and providing perfect forward secrecy using physsec on 8-bit  $\mu\text{c}$ ," in *2016 IEEE International Conference on Communications Workshops (ICC)*. IEEE, 2016, pp. 110–115.
- [28] C. Zenger, "Physical-layer security for the internet of things," 2017.
- [29] W. Tang, M. Z. Chen, X. Chen, J. Y. Dai, Y. Han, M. Di Renzo, Y. Zeng, S. Jin, Q. Cheng, and T. J. Cui, "Wireless communications with reconfigurable intelligent surface: Path loss modeling and experimental measurement," *IEEE Transactions on Wireless Communications*, vol. 20, no. 1, pp. 421–439, 2021.
- [30] I. Alamzadeh, G. C. Alexandropoulos, N. Shlezinger, and M. F. Imani, "A reconfigurable intelligent surface with integrated sensing capability," *Scientific Reports*, vol. 11, no. 20737, pp. 1–10, 2021.
- [31] Y. Xie, Z. Li, and M. Li, "Precise Power Delay Profiling with Commodity WiFi," in *The 21st Annual International Conference on Mobile Computing and Networking (MobiCom'15)*. New York, NY, USA: ACM, Sept. 2015, pp. 53–64, Paris, France.
- [32] M. Heinrichs and R. Kronberger, "Digitally tunable frequency selective surface for a physical layer security system in the 5 GHz Wi-Fi band," in *International Symposium on Antennas and Propagation (ISAP)*, Osaka, Japan, Jan. 2021, pp. 267–268.
- [33] L. Wu, K. Lou, J. Ke, J. Liang, Z. Luo, J. Y. Dai, Q. Cheng, and T. J. Cui, "A wideband amplifying reconfigurable intelligent surface," *IEEE Transactions on Antennas and Propagation*, vol. 70, no. 11, pp. 10623–10631, 2022.